Available online at www.sciencedirect.com
ScienceDirect
International Journal of Heat and Fluid Flow 28 (2007) 753–767
International Journal of HEAT AND FLUID FLOW
www.elsevier.com/locate/ijhff

Spray cooling heat transfer: The state of the art

Jungho Kim *

University of Maryland, Department of Mechanical Engineering, College Park, MD 20742, United States

Received 22 May 2006; received in revised form 11 September 2006; accepted 16 September 2006
Available online 13 November 2006

Abstract

Spray cooling is a technology of increasing interest for electronic cooling and other high heat flux applications, and is characterized by high heat transfer, uniformity of heat removal, small fluid inventory, low droplet impact velocity, and no temperature overshoot. The mechanisms by which heat is removed during spray cooling are poorly understood, however, due to its dependence on many parameters that are not easily varied independently, and predictive capabilities are quite limited. This paper provides an introduction to spray cooling for electronic cooling applications, reviews some proposed spray cooling heat transfer mechanisms, and summarizes the data regarding the effects of non-condensable gas, surface enhancement, spray inclination, and gravity. Some models of spray cooling are also presented.

Keywords: Heat transfer; Spray cooling; Electronic cooling

1. Introduction

Future electronic systems and power electronics will require increasing use of high heat flux removal technologies. In a study on the limits of device scaling and switching speeds, Zhirnov et al. (2003) conclude that "even if entirely different electron transport models are invented for digital logic, their scaling for density and performance may not go much beyond the ultimate limits obtainable with CMOS technology, *due primarily to limits on heat removal capacity*". High heat flux thermal designs are necessary to maintain lower operating temperatures, which increases the reliability of components and can result in higher performance. Some desired characteristics of these technologies are low cost, minimal power input, and adaptability to a wide range of heat fluxes. Use of liquid cooling will become unavoidable as the power dissipation levels increase in future electronic systems. Possible liquid cooling technologies include single-phase liquid cooling in microchannels, immersion flow boiling, spray cooling, jet impingement cooling, thermosyphons, and heat pipes. Each of the above has advantages and drawback which must be carefully weighed when selecting a system. Of the above cooling technologies, spray cooling appears to offer the best balance of high heat flux removal capability, isothermality, and fluid inventory.

It has also been shown by Cader et al. (2004) that the lower chip junction temperatures produced by spray cooling reduce transistor leakage currents, resulting in reduced power consumption and higher reliability. Test performed with dual Opteron Compact PCI computers resulted in a indicated a 33 °C reduction in junction temperatures and a 35% reduction in power consumption with a spray cooled system compared to an air-cooled version. Spray cooling is currently being used to cool the CRAY X-1 computer, and is a leading candidate to cool ground-based high-power diode laser arrays, future space-based lasers, and space-based radar.

Spray cooling is also used to selectively cool human skin during laser therapy of patients with port wine stain birthmarks (Basinger et al., 2004; Aguilar et al., 2003; Aguilar et al., 2001; Aguilar et al., 2001). It is desirable in this application to selectively target the blood vessels without causing excessive heating of the surrounding epidermis which

* Tel.: +1 301 405 5437.
E-mail address: kimjh@umd.edu

0142-727X/$ - see front matter © 2006 Elsevier Inc. All rights reserved.
doi:10.1016/j.ijheatfluidflow.2006.09.003

Nomenclature

$c_{p,l}$	specific heat of liquid
$c_{p,v}$	specific heat of vapor
d_0	nozzle orifice diameter
d_{32}	Sauter mean diameter
G	mass flow rate
h_{fg}	heat of vaporization
k	power
$\dot{m}$	mass flux
n	number
N	number flux
Nu	Nusselt number
P	pressure
Pr	Prandtl number
q	heat transfer
$\dot{q}''$	heat flux
r	radial distance
Re	Reynolds number
T	temperature
t	time
V	velocity
$\dot{V}''$	volumetric flux

Subscripts

f	fluid
l	liquid
sat	saturation
sub	subcooling
surf	surface
spray	spray
v	vapor
wall	wall

Greek symbols

η	efficiency
μ	dynamic viscosity
θ	spray cone angle
ρ	density
σ	surface tension

can lead to blistering, scarring, or dispigmentation. Heating of the epidermis poses an upper limit on permissible laser power that can be used with darker skin types. Short duration spray cooling is used to selectively cool the surface prior to laser exposure, allowing the use of higher energy pulses to thermally damage the deeper blood vessels.

Spray cooling occurs when liquid forced through a small orifice shatters into a dispersion of fine droplets which then impact a heated surface. The droplets spread on the surface and evaporate or form a thin liquid film, removing large amounts of energy at low temperatures due to the latent heat of evaporation in addition to substantial single-phase convection effects. Heat transfer rates much higher than can be attained in pool boiling are possible with sprays since there is less resistance to the removal of vapor from the heated surface. Other advantages include the possibility of uniformly cooling large surfaces, low droplet impact velocity, and no temperature overshoot. Some disadvantages include the need for pumps, filters, and the need to transport excess liquid and vapor to a condenser.

1.1. Nozzle types

Various types of sprays can be produced by specific nozzle types. Hollow-cones sprays are typically produced by forcing liquid tangentially into a swirl chamber or by grooved vanes directly upstream of an orifice. The swirling liquid exits the orifice as a ring of droplets. Full-cone sprays are produced by forcing liquid through stationary vanes that add turbulence. The shape of the spray can vary from circular to square to oval. Flat fan sprays are also available. Single spray nozzles can be used to cool a small area chip, or arrays of spray nozzles can be designed to cool larger areas.

Gas-atomizing nozzles use an air jet to help break up the liquid into finer droplets at higher velocity. The air jet also forms a stagnation point flow field, but the droplets do not follow the streamlines and impact the surface. The air jet is thought to thin the liquid film through shear forces, sweep away the vapor, and reduce the vapor partial pressure above the liquid film, enhancing evaporation.

Sprays typically consist of a wide range of droplet sizes. The parameter that is generally used to characterize sprays is the Sauter mean diameter, d_{32}, the droplet diameter with the same volume/surface ratio as the entire spray:

$$d_{32} = \frac{\sum n_i d_i^3}{\sum n_i d_i^2} \tag{1}$$

Although this diameter is useful in combustion or droplet evaporation studies where the energy released by chemical reaction or fuel volatilization is dependent on the surface area of the spray, it may not necessarily be the most appropriate for use in spray cooling heat transfer since the droplets impact the surface and form a thin film that evaporates. An estimate of d_{32} can be obtained from a correlation suggested by Estes and Mudawar (1995)

$$\frac{d_{32}}{d_0} = 3.07\left(\frac{\rho_v^{0.5}\Delta P d_0^{1.5}}{\sigma^{0.5}\mu_l}\right)^{-0.259} \tag{2}$$

The droplet velocity exiting the nozzle in liquid atomized sprays can be estimated from (Ghodbane and Holman, 1991)

$$V_0 = \left[V_{tube}^2 + \frac{2\Delta P}{\rho_l} - \frac{12\sigma}{\rho_l d_{32}}\right]^{1/2} \tag{3}$$

1.2. General aspects of the spray cooling curve

Spray cooling data are generally plotted as heat flux vs. wall temperature–an example is shown in Fig. 1 for spray cooling of a flat surface. At low wall temperatures, the curves are typically linear, indicating the heat transfer is dominated by single-phase convection, although some evaporation can also occur. Usually, the supply of cold liquid is so high (in order to maximize heat transfer) that there is little time for the heater to increase the local liquid temperature. Liquid is swept away by fresh cold liquid before it can heat up enough to generate a bubble. This suppression of nucleation due to the convective effect of liquid sweeping across a flat surface has also been observed in flow boiling by many researchers (e.g., Chen, 1966). High wall temperatures are required to begin significant bubble nucleation. Droplet impact onto the liquid film can also provide significant agitation, increasing the amount of heat transferred. As the superheat is increased, phase change becomes important as indicated by an increase in the slope of the spray cooling curve. Temperature overshoot has never been observed due to the entrainment of vapor or gas into the liquid film. As the heat transfer increases, dryout of the heater begins to occur outside the droplet impact area. Progressively larger fractions of the heater experience dryout until critical heat flux (CHF) occurs when the heat supplied to the heater just balances the liquid heat removal capability. CHF for spray cooling is typically much higher than for boiling since the vapor generated at the surface by phase change can be removed from the surface more easily.

1.3. Spray cooling efficiency

The efficiency with which the liquid is used to cool the surface can be characterized by the ratio of the CHF to the heat transfer capability of the fluid. The spray efficiency is generally defined as

$$\eta = \frac{\dot{q}''}{\dot{m}''[c_{p,l}(T_{sat} - T_{spray}) + h_{fg}]} \tag{4}$$

and accounts for sensible heating of liquid from the spray impact temperature (it should be noted that this temperature may be significantly different from the temperature of the liquid exiting the spray nozzle) to the saturation temperature (T_{sat}) and the heat required to vaporize the liquid. However, this definition makes no allowance for heat transfer to the vapor. Since the vapor generated at the surface can be superheated to the wall temperature, a more appropriate definition of spray efficiency is given by

$$\eta = \frac{\dot{q}''}{\dot{m}''[c_{p,l}(T_{sat} - T_{spray}) + h_{fg} + c_{p,v}(T_{wall} - T_{sat})]} \tag{5}$$

Spray efficiency defined by Eq. (4) will be used in this paper due to its widespread use unless stated otherwise.

If the liquid mass flux striking the heater is small, all of the liquid can evaporate and the liquid is utilized very efficiently. The surface heat transfer, however, is generally quite low. Although heat transfer increases with mass flux, spray efficiency generally decreases as illustrated in Fig. 2.

1.4. Objectives

The purpose of this paper is to introduce the reader to the capabilities of spray cooling for electronic cooling applications, review current understanding of spray cooling mechanisms, and to outline areas where additional research is needed. Although heat transfer at high temperatures where a vapor film forms between the hot wall and the liquid has been studied extensively (e.g., for cooling of steel in strip mills), this regime is generally not of interest to electronic cooling and is not discussed in this paper. The reader

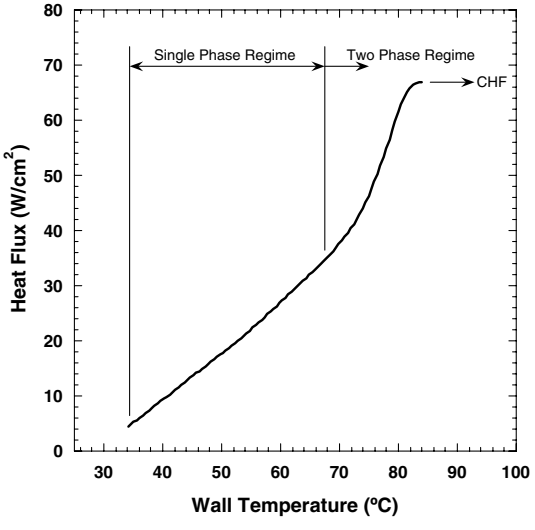

Fig. 1. Typical spray cooling curve (FC-72, 93 ml/min, 1.0 bar, $T_{sat} = 57$ °C, $\Delta T_{sub} = 28$ °C, 2 cm^2 copper heater).

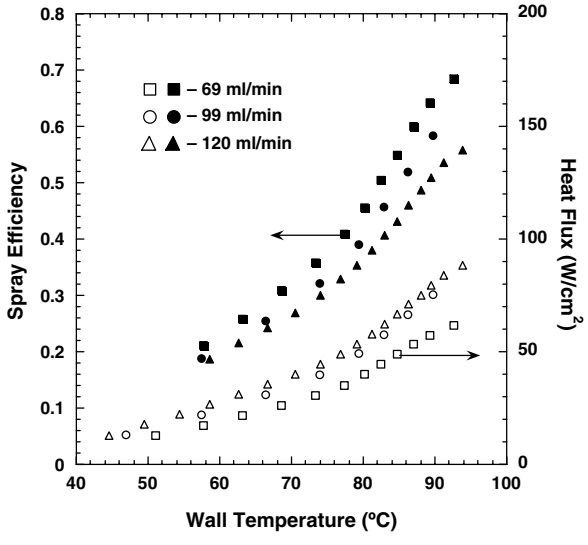

Fig. 2. Spray efficiency (Eq. (5)) and heat transfer vs. wall temperature (FC-72, 2 cm^2 flat copper heater, $T_l = 29.6$ °C, 1.0 bar, $T_{sat} = 57$ °C).

is referred to many of the excellent papers on this topic (e.g., Toda, 1974; Liu et al., 2000). This paper also does not address heat transfer mechanisms during droplet cooling (individual droplets striking a dry, hot wall) primarily because the heat transfer signature of individual droplets cannot be extrapolated to predict spray behavior where the individual droplets generally strike a liquid film. The droplets in these studies are also generally much larger than the droplets within sprays. Droplet cooling mechanisms might be applied to very sparse sprays, but the heat transfer would be very low and therefore not applicable for electronic cooling. Interested readers are referred to the droplet cooling papers given in di Marzo et al. (1993), Milke et al. (1997), Qiao and Chandra (1997), Bernardin et al. (1997), Bernardin et al. (1997), Qiao et al. (2000), Lee et al. (2001), Lee et al. (2000), Lee et al. (2002).

2. Spray cooling of flat surfaces

The mechanisms by which heat is removed during spray cooling are very complex due to its dependence on many factors. The droplets produced by spray nozzles have unique droplet size distributions, droplet number density, and velocities that change with the liquid flow rate (pressure drop across the nozzle) and nozzle geometry. Unfortunately, it is very difficult to vary each of the above parameters independently so their effects are not easily measured. Other factors affecting spray cooling heat transfer are impact angle, surface roughness, gas content, the presence of other nozzles and walls, and heater surface orientation.

2.1. Heat transfer mechanisms in the single-phase regime

The spray cooling curve has been observed by many researchers to be quite linear at low superheats, indicating that single-phase convection is the primary heat transfer mechanism. Pautsch and Shedd (2006) verified this using a novel technique to measure the local film thickness produced by sprays. They used a transparent ITO heater deposited on a 0.5 mm thick glass die as the heater. The side of the die that did not have the ITO was coated with a thin layer of paint to form a light diffuser. Illumination of the paint with a laser produced a diffuse point source of light. When the scattered light hit an interface at incident angles less than the critical angle, most of the light was transmitted and a small part was reflected. At the critical angle and beyond, all light was reflected back to the outer wall, forming a light ring around the point source. The diameter of the light ring (~0.75 mm) was proportional to the total distance the light travels on its round trip through the die and liquid. They verified that this system could be used in the highly disturbed, wavy film produced by sprays with a claimed spatial resolution of 0.6 mm and film thickness uncertainty of 0.7 μm through time averaging. The film thickness was found to remain constant when a heat flux of 15 W/cm^2 was applied, indicating that the heat transfer mechanism was dominated by single-phase convection.

Heat transfer increases with increasing flow rate for a number of reasons. A larger fluid flow results in higher liquid velocity over the surface and a thinner thermal boundary layer, similar to what is observed in jets. The impact of the droplets onto the film can also agitate the liquid, thinning the thermal boundary layer locally.

Little research has been performed on correlating single-phase data and prediction capabilities are limited. Rybicki and Mudawar (2006) used d_{32} and volumetric flux as length and velocity scales, respectively, and suggested the following correlation in the single-phase regime for PF-5052:

$$Nu = 4.70 Re^{0.61} Pr_f^{0.32} \tag{6}$$

where $Nu = \frac{\dot{q}''}{T_{wall}-T_l}\frac{d_{32}}{k_f}$ and $Re = \frac{\rho_f \dot{V}'' d_{32}}{\mu_f}$. This correlation has yet to be verified by other researchers and for other fluids.

2.2. Heat transfer mechanisms in the two-phase regime

Numerous mechanisms have been proposed in the two-phase regime. A summary of the proposed mechanisms is given below.

2.2.1. Thin film evaporation

Pais et al. (1989) and Tilton (1989) suggested that the high heat transfer observed in spray cooling was due to the efficiency by which liquid molecules escape into the vapor/ambient at the surface of a thin liquid film. The suggested a thin liquid layer forms on the heated surface through which heat is conducted. Because the top of the film is assumed to be at the saturation temperature, thinner films result in higher heat transfer. Large heat transfer at small superheats requires the existence of an ultrathin liquid film on the surface. For example, a 1.4 μm thick layer of water is required to transfer 1000 W/cm^2 of heat at a superheat of 20 °C. Their analytical model suggested that the optimum heat transfer would occur by using the smallest possible droplets and the highest percentage of surface saturation to obtain the thinnest liquid film. They also suggested that the impact velocity should be carefully chosen such the maximum droplet spread is achieved without droplet rebound from the surface.

2.2.2. Secondary nucleation

Yang et al. (1996) used an air-atomized nozzle to spray distilled water over an area approximately 12 mm in diameter. The heater surface was constructed of copper with an exposed area of 11 × 11 mm^2. Water flow rates up to 3 l/h were used. The droplet diameters and velocities ranged from 10–18 μm and 25–58 m/s, respectively. Heat fluxes of about 820 W/cm^2 were achieved at a flow rate of 2 l/h and an air pressure of 446 kPa. They suggested that the observed high heat transfer was due to the generation of many nucleation sites within the liquid film that form when

the individual liquid droplets strike the liquid surface. The droplets have a layer of gas molecules adsorbed onto the surface. When these droplets penetrate into the liquid film, the gas is released and form nucleation sites from which bubbles can grow. The droplets can also puncture the rapidly growing bubbles, increasing the bubble frequency and the heat transfer. Although the number of nucleation sites is proportional to the droplet flux (the liquid flow rate), the heat transfer is not proportional to liquid flow rate since the liquid film thickness also increases.

Rini et al. (2002) used a $1 \times 1 \times 0.05$ cm^3 semi-transparent synthetic diamond film with a Ni–Cr resistor deposited on the underside as the heater surface. A thermocouple measured the temperature at the underside of the diamond film. Degassed FC-72 was used to cool the surface. Visualization of the droplet impact and bubble behavior was obtained using a high-speed camera at framing rates up to 8000 fps and shutter speeds of 1/80,000 s. Image processing of the individual frames was used to determine the bubble growth rates and the bubble site density. They observed nucleation site densities ranging from 1000/cm^2 to over 4000/cm^2, which was significantly more than typically observed in pool boiling. For example, the nucleation site density was about 900/cm^2 at 68 °C during pool boiling on the heater (10 W/cm^2), but increased to 3500/cm^2 during spray cooling at 67 °C (60 W/cm^2). The bubble density also increased as the droplet number flux increased. Bubble growth curves indicated that the bubbles grew as $t^{1/2}$ (heat transfer controlled regime) similar to what was observed in pool boiling, but the bubbles were punctured earlier in their growth cycle by the incoming droplets. The bubble lifetimes during spray cooling were more than an order of magnitude smaller than during pool boiling. Although early removal of the bubble was speculated to increase heat transfer as might be expected from pool boiling studies, this was not found to be the case, probably because the bubbles were not attached to the wall. The authors felt that the increase in heat transfer with number flux was attributable to turbulent mixing within the film increasing convection and direct evaporation.

2.2.3. Contact line heat transfer

Horacek et al. obtained time and space resolved heat transfer distributions produced by a single nozzle (Horacek et al., 2005) and two interacting nozzles (Horacek et al., 2004) using an array of individually controlled microheaters, while visualization and measurements of the liquid–solid contact area and the three-phase contact line length were made using a Total Internal Reflectance (TIR) technique (Fig. 3). An ISR spray nozzle was used to spray FC-72 containing varying amounts of non-condensable gas onto a microheater array with total area of 0.49 cm^2 (7.0 mm × 7.0 mm). The nozzle-to-heater spacing was 17 mm, and resulted in the entire heater surface covered by spray. The flow rate impacting the heater was 11.3 ml/min at a velocity of about 21 m/s.

Statistical quantification of the images was possible through the identification of various geometrical characteristics of the wetted surface, such as the wetted area fraction and the contact line length density (CLL). The average fraction of the heater surface wet by liquid as a function of wall superheat indicated that the wetted area fraction monotonically decreased as the wall superheat increased. The amount of liquid on the surface appeared to correlate with wall superheat but not with wall heat flux. However, the data indicated that CLL increased with superheat, reached a maximum at the superheat where CHF occurred, then decreased as the surface dried out. The curves' shapes were very similar to the heat flux profiles, indicating a strong correlation between CLL and heat transfer. The relationship is illustrated by plotting CLL against heat flux (this has been corrected for sensible heating) as shown in Fig. 4. CHF occurs at the highest CLL density. The similarity in the CLL and heat flux curves indicates that the phase-change contribution to heat transfer is directly proportional to the CLL. It is unknown at this time whether heat is transferred at the contact line by the thin film heat transfer mechanisms suggested by Wayner (1999) or by an alternate mechanism such as transient conduction into the liquid as it moves over the surface as has been proposed for pool boiling (Demiray and Kim, 2004). Further

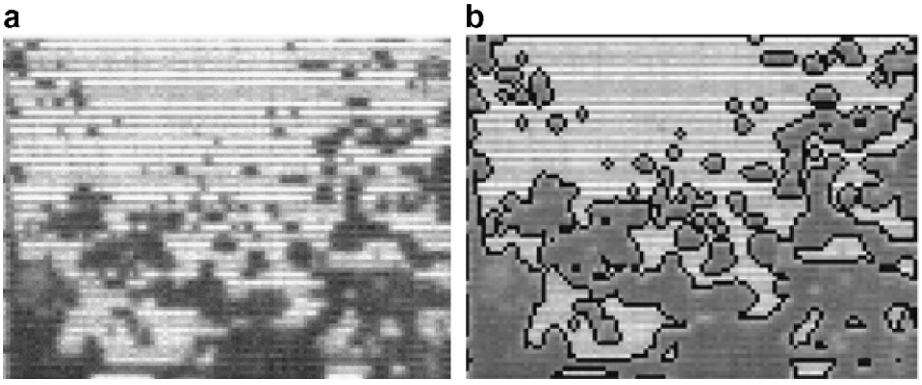

Fig. 3. Sample image of surface liquid vapor distribution obtained using TIR and the image processing sequence: (a) Original image and (b) final detected edges superimposed on original image.

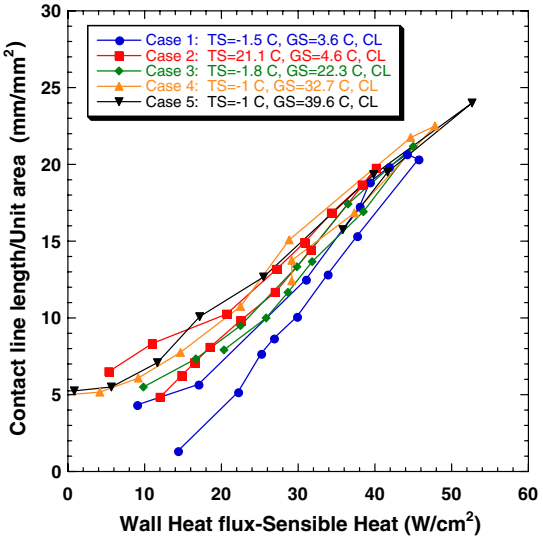

Fig. 4. Variation of the average contact line length for the center eight heaters in the array with the wall heat flux.

experiments which directly manipulate the contact line length in both a static and dynamic configuration are needed to elucidate which of these mechanisms is correct.

2.3. Critical heat flux

The mechanisms by which CHF is triggered during spray cooling are currently not known. CHF is generally thought to occur first outside the spray impact region then propagate inward as the wall temperature increases. Two possible mechanisms include homogeneous nucleation within the film, and liftoff of the thin liquid layer due to nucleation within the film.

Mudawar and Estes (1996) obtained CHF data using a Spraying Systems full-cone spray nozzles to cool a copper surface $12.7 \times 12.7\ \text{mm}^2$ surface with FC-72 and FC-87. They argued that the volumetric flux and not the mean droplet velocity is the proper scaling factor for heat transfer correlations near CHF since the mean velocity fails to account for the droplet number flux. They found that the volumetric flux striking the surface could be predicted using purely geometric considerations for the nozzle used. At small nozzle-to-surface distances, the spray impact area was small and only a small fraction of the heater area was cooled, resulting in low CHF values. CHF increased as the nozzle-to-surface distance increased, and peaked when the spray impact area just inscribed the heater surface. Lower CHF values were observed at larger distances due to overspray. Based on CHF data on impinging jets (Monde et al., 1980), they argued that CHF should scale according to the Weber number, density ratio, and the Jakob number. The Weber number was based on the volumetric flux of liquid and d_{32}. The correlation presented is given as

$$\frac{\dot{q}''}{\rho_v h_{fg} \dot{V}''} = 1.467[(1+\cos(\theta/2))\cos(\theta/2)]^{0.3} \left(\frac{\rho_l}{\rho_v}\right)^{0.3} \left[\frac{\rho_l \dot{V}''^2 d_{32}}{\sigma}\right]^{-0.35} \times \left[1 + 0.0019 \frac{\rho_l c_{p,l} \Delta T_{sub}}{\rho_v h_{fg}}\right] \quad (7)$$

and accounts for flow rate, drop size, fluid properties, and subcooling. The claimed uncertainty is ±30%. Estes and Mudawar (1995) validated this equation for water as well, although some of the water data at high volumetric fluxes ($5 \times 10^{-3}\ \text{m}^3/\text{m}^2\ \text{s}$) and subcooling ($\Delta T_{sub} = 77\ ^\circ\text{C}$) were well outside the ±30% uncertainty range.

2.3.1. Effect of impact velocity, d_{32}, and number flux

The effects of droplet size, droplet flux, and droplet velocity on the heat transfer coefficient and CHF were studied by Chen et al. (2002, 2004) using water. They tested more than 20 full-cone nozzles from Hago (B-series nozzles), Bete, and Delavan, and generated test data at about 3000 combinations of d_{32}, V (droplet velocity), and N (mean droplet flux $= nV$ where n is the droplet number density) by varying the pressure across the nozzles and the distance from nozzle exit to the heater. The above parameters were measured using a Dantec PDPA. The uncertainty in both V and d_{32} were estimated to be 5%, while the uncertainty in N was estimated to be accurate within 30%. The mass flux G (kg/s) computed from the PDPA measurements according to

$$G = \frac{1}{6}\rho\pi d_{32}^3 nV = \frac{1}{6}\rho\pi d_{32}^3 N \quad (8)$$

agreed with direct measurements using a stopwatch and graduated cylinder to within 10%. Data mining techniques were then used to compare cases where two of the parameters were similar while the third varied.

The effect of N is illustrated in the data presented in Table 1. N varies by a factor of 4.2, while d_{32} and V were kept within 56 μm ± 2% and 7.5 m/s ± 7%, respectively. As N increased, CHF increased by 30%. Similar data where N increased by a factor of 3.2 from $5.52 \times 10^6\ (\text{cm}^2\ \text{s})^{-1}$ to $17.4\ (\text{cm}^2\ \text{s})^{-1}$ while d_{32} and V were kept within 76 μm ± 5% and 10.5 m/s ± 5%, respectively indicated an increase in CHF from 591 W/cm² to 695 W/cm², then a decrease to 673 W/cm², about a 17% increase.

Similar data illustrating the effect of d_{32} on CHF indicated that varying d_{32} by a factor of 3 produced CHF values within 5%. An increase in d_{32} by a factor of 3 while N and V are kept constant produces a 27 factor increase in

Table 1
Effect of N on CHF (data from Chen et al., 2002)

Nozzle type	B37	B50	Bete #2
N (1/cm² s)	7.3×10^6	15.3×10^6	29.0×10^6
d_{32} (μm)	57.3	55.4	54.7
V (m/s)	6.9	7.3	8.0
CHF (W/cm²)	611	762	780

Table 2
Effect of V on CHF (data from Chen et al., 2002)

Nozzle type	B150	B200	Bete #3
N (1/cm^2 s)	16.4×10^6	13.5×10^6	15.1×10^6
d_{32} (μm)	67.2	70.2	68.7
V (m/s)	4.64	5.97	24.1
CHF (W/cm^2)	637	645	946

mass flux, and illustrates that mass flux can vary tremendously with little variation in CHF.

The effect of droplet velocity is illustrated using the data shown in Table 2. Both d_{32} and N were kept within 68.0 μm ± 2% and 15.0×10^6 (cm^2 s) ± 10%, respectively while V was increased by about 40%. CHF was observed to increase by about 49% over this range. Because both droplet flux and d_{32} were constant, the mass flux only varied by about 5%.

These results indicate that droplet velocity (V) had the largest impact on CHF followed by the droplet flux (N). The droplet diameter had negligible effect. A dilute spray with large velocity was found to be more effective than a dense spray with low velocity. The conclusions of this study contradict those of Mudawar and Estes (1996).

2.4. Summary of flat plate spray cooling

The complexity of the spray cooling process has resulted in significant disagreement regarding the fundamental mechanisms of spray cooling heat transfer. Although it is evident that single-phase heat transfer is dominant at low temperatures, the relationship between the spray parameters and the heat flux is not understood. Reliable correlations based on spray parameters are needed. The partitioning of energy between single-phase and two-phase mechanisms at higher wall temperatures and the mechanisms by which CHF occurs also needs further investigation.

3. Spray cooling of enhanced surfaces

3.1. Surface roughness effects

Sehmbey et al. (1990) investigated the effect of surface roughness using an air atomizing nozzle to spray water onto a 9 × 9 mm^2 heating surface. Two surface roughnesses were prepared on a copper surface in one direction using either 14 μm grit emery paper or the 14 μm grit emery paper in conjunction with a 0.3 μm grit polish. The surface profiles were measured using a diamond profilometer. With a water flow rate of 4.0 l/h and an air flow rate of 0.25 l/s, the heat flux for the smoother surface resulted in 40–50% increase in heat transfer when the surface temperature was above 80 °C. The authors attributed this effect to a lower conduction resistance on thinner liquid film, and also to a decrease in vapor pressure at the free surface caused by the air flow field. The maximum heat flux achieved was in excess of 750 W/cm^2. Heat fluxes up to 1250 W/cm^2 at very low superheats were observed in a follow-on study by Pais et al. (1992) on ultrasmooth copper surfaces. Evaporation from the thin film was stated to be the dominant heat transfer mechanism for this surface.

Ortiz and Gonzalez (1999), observed the opposite trend. They cooled 1.25 cm diameter copper surfaces roughened using either 600 grit SiC grinding paper or a 0.25 μm polycrystalline diamond suspension. The rough surface had higher CHF than the smooth surface at all flow rates tested (1.48 –2.9 l/h). CHF on the rough surface was up to 100% higher than on the smooth surface at lower flow rates, but this enhancement decreased to 15% at the highest flow rate. CHF was also delayed to higher wall temperatures on the rough surface.

3.2. Microstructured and microporous surfaces

Heat transfer on microstructured and microporous surfaces with dimensions much larger than the roughness studied by Sehmbey et al. (1990) was studied by Stodke and Stephan (2005) using water and a full-cone spray atomizer (60° cone angle, impact velocity ~11 m/s, $d_{32}\sim100$ μm). Pyramidal microgrooves 75 μm high with 150 μm pitch were manufactured onto a 20 mm diameter copper cylinder. The micropyramids had the same height and base length as the microgrooves. Both microstructured surface increased the wetted area by $\sqrt{2}$. The porous layer was 100 μm thick and created using a mixture of MEK, epoxy, and aluminum powder with an average size of 35 μm. Although little increase in heat transfer was observed for both microstructured surfaces at a standoff distance of 25 mm (highest mass flux), very large increases were observed when the standoff distance was increased. A maximum heat transfer of 97 W/cm^2 was observed at a standoff distance of 35 mm for the micropyramid surface compared with 30 W/cm^2 on the flat surface at a superheat of 12 °C, which was much larger than the surface area enhancement. Significant degradation in heat transfer for the microporous surface was observed compared with the uncoated surface due to the poor thermal conductivity of the epoxy binder. This is in contrast to the results obtained by Kim et al. (2004) who found that the heat transfer from microporous coated surface increased 50% relative to the uncoated surface. Their mass fluxes, however, were very small (maximum flow rate was 1.5 ml/cm^2-min) so the conduction resistance of the coating was probably not significant. The maximum heat flux achieved was 3.2 W/cm^2.

Hsieh and Yao (2006) and Amon et al. (2005) studied the heat transfer on square microstuds (160–480 mm size, groove depths 333–455 μm, groove widths 120–360 μm) manufactured on silicon. Two full-cone pressurized spray nozzles (60° and 80° cone angles, flow rates up to 4.41 ml/cm^2 min, d_{32} between 75 and 100 μm) were used to spray water at very low flow rates onto the surfaces. Surface texture was found to have little effect in the single-phase and dryout regimes. The authors attributed the

higher heat transfer observed for the microtextured surfaces in the intermediate regimes to more effective spreading of the liquid by capillary forces. A plain aluminum surface was found to have higher heat transfer than a silicon surface, but this disadvantage could be overcome by surface texturing. The maximum heat flux achieved was just over 50 W/cm^2.

3.3. Surface geometry

The effect of surface geometry has been studied by Silk et al. (2004). A Parker Hannifin spray plate containing a 2×2 array of hollow-cone nozzles (volume flux = 0.013 m^3/m^2 s) was used to spray FC-72 onto the three structured surfaces shown in Fig. 5 fabricated on a copper rod 1.60 cm in diameter (2.0 cm^2 projected area). The wetted area of the cubic pin fins and the straight fins was 4.0 cm^2 while the pyramids had a wetted area of 4.5 cm^2. If the heat flux were to scale with the total wetted area, then the pyramid surface should have the highest heat transfer with the cubic pin fins and straight fins having similar but intermediate heat flux magnitudes.

The heat flux data for the degassed case is shown in Fig. 6. The spray cooling curves for all four surfaces are linear at low wall temperatures, indicating single-phase heat transfer. The performance of the pyramid, cubic pin fin, and straight fin surfaces all exceeded that of the flat surface, but the straight finned geometry performed best with CHF exceeding that for the flat surface by 45 W/cm^2 (a 55% increase). The data indicated that the heat transfer does not scale directly with the total wetted surface area. It was speculated that the straight fins yielded the higher heat fluxes due to greater surface flow confinement effects. Surface geometries that have acute angles relative to the base (i.e., pyramids) can be considered less effective in constraining the fluid flow on the heater surface.

3.4. Heat transfer on straight fins

Additional investigation into the heat transfer on straight finned surfaces machined into copper was performed by Coursey et al. (2006). A single ISR full-cone spray nozzle (31° cone angle, 69–123 ml/min) was used to spray FC-72 onto straight finned structures fabricated on the surface of a copper block with 1.41×1.41 cm^2 cross section. The fins were 500 μm wide with a pitch of

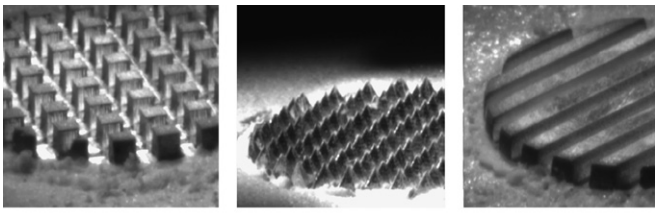

Fig. 5. Enhanced surfaces tested.

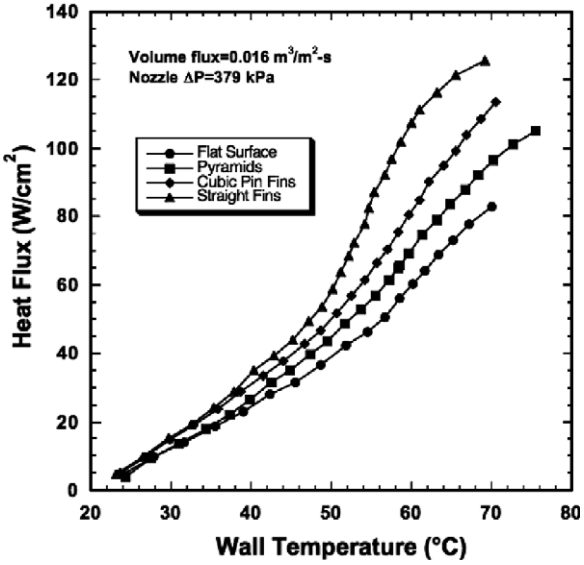

Fig. 6. Spray cooling curves for the geometries tested. The heat flux is based on the projected area (2.0 cm^2).

860 μm. The fin height varied from 0.25 mm to 5 mm. The nozzle was fixed 18 ± 1 mm above the heated wall (i.e., the base of the fins for the finned surfaces), which resulted in a spray that appeared to approximately inscribe the base of the test surface.

Spray cooling curves for the six test surfaces are shown in Fig. 7. A significant performance enhancement is observed for each of the five enhanced surfaces at all nozzle pressures compared to the flat surface. As expected, increasing the nozzle pressure (and therefore mass flux) resulted in higher heat transfer. Furthermore, there were distinctly different trends in the single-phase and two-phase regimes. In particular, the finned surfaces showed a significant enhancement in the total heat flux once two-phase effects began. Although CHF was observed for the flat surface, CHF was not reached for most of the finned surfaces due to the heating block reaching temperatures greater than the safe temperature limit of the test apparatus.

3.4.1. Single-phase results

In the single-phase regime, the 5 mm long fins provided the best enhancement and the 0.25 mm fins the least. Although the total surface area increased linearly with fin length, the heat transfer enhancement appeared to asymptotically approach an optimum value at a fin length slightly longer than 5 mm. The results observed in the single-phase regime are due to a number of competing mechanisms. Adding fin length not only increases the wetted area, but also increases the amount of fluid incident on the surface since the top of the fin structure intercepted a larger fraction of the spray. There two effects are offset by the addition of conduction resistance within the fin, less uniform distribution of liquid due to more channeling, and heating of the fluid as it travels down the fins (lower local ΔT near the bottom of the fins).

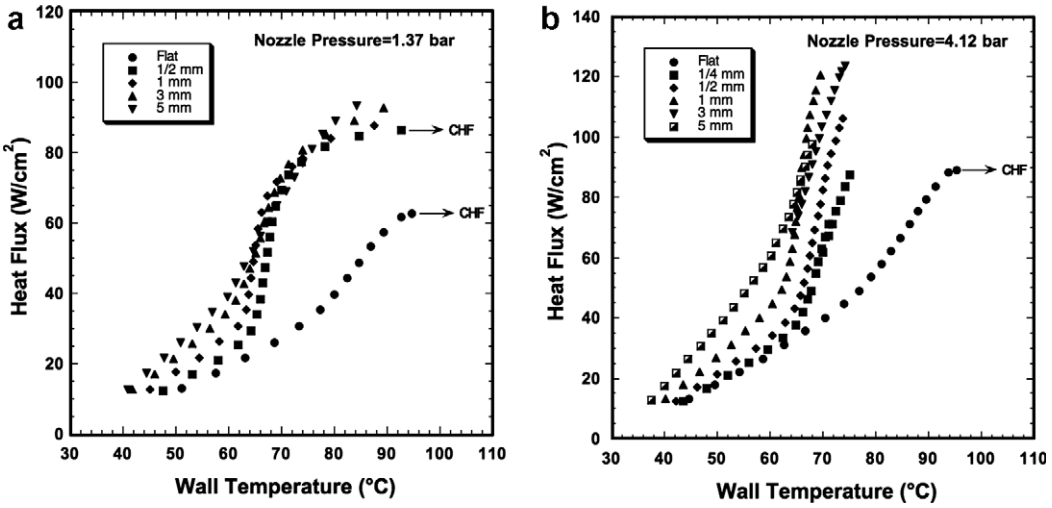

Fig. 7. Spray cooling curves for 1.37 bar (20 psig) and 4.12 bar (60 psig) nozzle pressure.

3.4.2. Two-phase results

The finned surfaces enter the two-phase regimes at temperatures closer to the saturation temperature. This may be due to an increase in the number of potential nucleation sites due to increased area, a longer residence time as the liquid must travel down the fin and out of the channel before leaving the hot structure, or channeling of the liquid leaving the inner channels with sufficient liquid but the outer channels partially starved. Furthermore, liquid pooling may occur on the portions of the fin that are shaded from the impinging droplets, allowing nucleation to occur more easily. It is also noteworthy that the temperature at which two-phase effects become dominant is independent of flow rate, and may indicate that geometry rather than residence time is responsible for the earlier onset of two-phase effects on finned surfaces.

Another interesting aspect of the two-phase regime is the delayed transition toward CHF observed in the 1.36 atm (20 psig) tests. The finned surfaces begin to show a decrease in their heat transfer coefficients around 71 °C although CHF is not reached until over 90 °C, indicating that dryout occurs gradually. This may be due to channeling of the spray, which allows the outer channels with less liquid to begin drying out before the fluid rich center channels.

The spray efficiencies (defined according to Eq. (5) are shown as a function of temperature in Fig. 8. The mass flow rates used are based on the flow incident on the top surface of the finned structure. While the spray efficiencies of the flat surface are characteristically low, the efficiencies of the finned structures appear to approach unity. This trend is particularly evident in the 1.36 atm (20 psig) data. In the single-phase regime, efficiencies increase as fin length increases, although the efficiencies are still rather low because there is no latent heat transport. The onset of two-phase effects corresponds to a large increase in the spray efficiency, and since the onset occurs at different temperatures for different channel heights the optimum fin length varies with temperature.

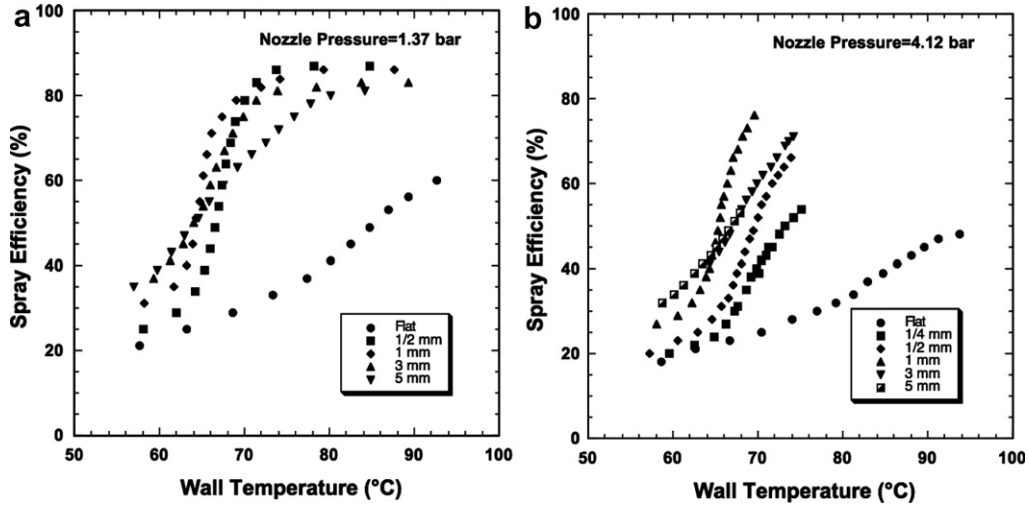

Fig. 8. Spray efficiency as a function of wall temperature for 1.37 (20 psig) and 4.12 bar (60 psig) nozzle pressure difference.

These findings indicate some important results. The efficiencies of the finned surfaces for the 1.36 atm (20 psig) pressure difference collapse onto a single curve as CHF is approached, and this single curve indicates almost total evaporation of the incident spray. By channeling the spray and forcing liquid to travel down the fins and through the microchannels, it has sufficient residence time to heat up to the wall temperature in the single-phase regime, or to the saturation temperature and completely evaporate in the two-phase regime. The very high spray efficiencies observed in this study are likely due to the small scale of the microchannels along with the relative sparseness of the spray. It is likely that a greater flow rate would result in improved heat transfer, but at the expense of decreasing spray efficiency. However, spraying microchannels with a sparse spray may be one way of improving thermal performance without increasing the mass flow rate, which can be expensive in terms of pump power, cost, and weight.

3.5. Summary of enhanced surface spray cooling

Much higher heat flux for a given liquid flow rate can be achieved by the addition of roughness elements larger than the liquid film thickness. Enhancing the surface promotes the onset of two-phase effects at wall temperatures lower than on flat surfaces, leading to improved heat transfer coefficients at lower wall temperatures. CHF is higher than for flat surfaces, and is approached much more gradually. The combination of high heat removal at low temperature, high spray efficiency, and the graceful approach to CHF make the use of enhanced surfaces highly attractive for electronics cooling applications. The mechanisms are not yet understood.

4. Other effects

4.1. Non-condensable gas effects

Relatively little research has been performed regarding the effects of dissolved gas on spray cooling heat transfer. It has been suggested that the presence of a non-condensable gas degraded the condenser performance to the point where excess fluid removal was inhibited (Tilton et al., 1992). It was noted that for fixed volume systems, the presence of gas would cause the boiling temperature to increase, increasing the surface temperature. A more recent study by Lin and Ponnappan (2003) indicated that while dissolved gas indeed degraded the performance at lower wall temperatures, the maximum heat transfer increased compared to sprays without dissolved gas. The two main effects of dissolved gas on sprays were to shift the spray cooling curves to higher temperatures and to increase CHF. In this study, four fluids (FC-87, FC-72, methanol, and water) were used. It was found that air accidentally introduced into the system during a test with FC-72 caused the spray cooling curves to shift to higher wall temperatures, but CHF also increased from about 70 W/cm^2 without air ($P = 0.295$ bar) to 91 W/cm^2 with air ($P = 0.85$ bar). They attributed the better thermal performance with gas to two effects. They stated that air sprayed on the surface along with the liquid causes the liquid droplets to be smaller and have higher velocity, resulting in a thinner liquid film on the surface. The air flow field was also thought to replace the evaporating vapor and lower the partial pressure over the liquid film, enhancing evaporation.

Horacek et al. (2005) obtained spray cooling curves with varying amounts of dissolved air in FC-72 and confirmed the observations of Lin and Ponnappan (2003). They found that if the temperature scale was plotted in terms of the wall superheat, CHF occurred at similar superheats, and much of the difference in the CHF values could be accounted for if sensible heat contribution was considered. They attributed the remaining effects to additional single-phase convection over the heater areas not covered by drops, additional evaporation of the liquid, nucleation of bubbles within the drops or thin film spreading the liquid over a larger heated area.

4.2. Effect of spray inclination

Studies where the spray is inclined relative to the heated surface indicate that there is little effect unless the inclination angle significant. Schwarzkof et al. (2004) used a single spray nozzle to cool a heated surface using PF5060 at a flow rate of 22 ml/min. The inclination angle was varied between 0° and 60° with the nozzle located a fixed radius of 1.4 cm from the center of the target. The cooling capability dropped off significantly when the angle exceeded 40°.

When multiple nozzles are used to cool a larger surface, stagnation regions between the nozzles where liquid accumulates can form. Stagnation regions can also occur in the region directly under hollow-cone spray nozzles. Recent studies have indicated that inclining the spray axis relative to the heater can result in higher heat transfer by eliminating the stagnation zones (Silk et al., 2005). When PF-5060 was sprayed onto a 1 cm^2 flat copper surface (78 ml/cm^2 min) using a 2×2 nozzle array, CHF increased by 24% as the spray inclination angle increased from 0° to 45°.

4.3. Large area heat transfer

Almost all of the available spray cooling data are for cooling of surfaces less than 2 cm^2 using single nozzles or a small array of nozzles. Little data exists for cooling of larger areas using multiple nozzles. Lin et al. (2004) studied spray cooling of a 19.3 cm^2 (2.54×7.6 cm^2) surface using an array of 4×12 miniature nozzles (0.25 mm orifice diameter, 35.2°spray cone angle) with FC-72. The distance between the spray plate containing the nozzles and the heater surface was 10 mm. Each of the nozzles in the array was designed to cool an area 6.35 mm in diameter. Dissolved

gas was removed from the system before testing. The maximum heat flux observed for the large area was 59.5 W/cm^2 with the heater in a horizontal facing downward position. CHF with the heater in a vertical position was about 5% lower. A 2.0 cm^2 heater cooled by an eight nozzle array and a similar mass flux had CHF values about 30% and 34% higher than for the larger heater, depending on the orientation. It is currently not known why the larger area has lower heat transfer, but the authors speculated that it was due to the difference in interaction between the spray droplet and the vapor/excess liquid flow. The center excess liquid could not be discharged to the side, resulting in a thicker liquid film and lower heat transfer. Additional studies are needed to elucidate the reasons for the heat transfer degradation.

4.4. Gravity effects on spray cooling

Because the drops within the spray generally have large momentum, spray cooling is not expected to be affected by heater orientation relative to the gravity vector, or by low gravity conditions.

Low-g effects were studied by Yoshida et al. (2001) who obtained cooling curves with water and FC-72 in the low-g (0.01 g) and high-g (1.8 g) environments produced by aircraft flying parabolic trajectories. Copper blocks (the heater surface was 50 mm in diameter) were heated to above the Leidenfrost point, then cooled with a spray to generate data from film boiling regime through the nucleate boiling regime. The maximum volume flux of water (2.22 ml/cm^2 min) and FC-72 (1.35 ml/cm^2 min) tested were very low. Earth gravity data with the heater and nozzle in various orientations were also obtained. No effect of gravity was observed in the nucleate boiling regime and CHF. They did observe significantly lower heat transfer in the transition boiling regime and at minimum heat flux in the low-g environment and downward facing heaters (earth gravity) than for the upward facing heater (earth gravity) due to the lack of secondary impact from droplets that had rebounded from the surface.

Low-g environments can dramatically affect spray cooling at higher flow rates if the surface becomes flooded due to inefficient removal of excess liquid. Surface tension flow around the spray nozzle leading improper atomization has been observed (Baysinger et al., 2004).

5. Mechanistic modeling of spray cooling

It is currently not possible to model the spray cooling process (droplet formation, droplet flight, impact onto the liquid film, and the resulting single-phase and two-phase heat transfer) from first principles due to the enormous number of droplets. Submodels that attempt to capture the heat transfer due to impinging droplets onto a heated surface have been attempted, however.

Chen et al. (2005) attempted to simulate FC-72 spray cooling heat transfer at 4 °C superheat by tracking the lifetime of many bubbles nucleating within a liquid film. It was assumed that bubbles nucleated at fixed sites randomly located (but spaced at least 350 μm apart) or at multiple secondary nucleation sites around droplets impacting the liquid film. All nucleating bubbles were assumed to grow according to $t^{1/2}$ and left the surface when they grew to a certain size, or were punctured by incoming droplets. Bubbles could also merge together and form larger bubbles. Simulations were performed using various time steps, number of fixed and secondary nuclei, and bubble growth rates. The authors concluded that fixed-site nucleation was not an important factor. The results were sensitive to the number of secondary nuclei generated per droplet and bubble growth rate. The numerical results were within the range of the experimental observations.

Shedd and Pautsch (2005) and Pautsch and Shedd (2005) studied spray cooling of a Multi-Chip Module (MCM) using single and multiple nozzles manufacture by Parker Hannifin. Nitrogen saturated FC-72 at 1 atm was used as the working fluid. Heat transfer measurements were obtained by using the silicon die, while flow visualization was obtained by replacing the MCM with a clear acrylic substrate containing electrically powered, ITO-coated glass heaters. The formation of a cross-like drainage flow pattern was seen in multi-nozzle operation. They partitioned the heat transfer into a single-phase dominated regime in and around the droplet impact region, a two-phase liquid film boiling component away from this region, and a single-phase liquid drainage flow component between nozzles when multiple nozzles were used. Their dimensional equation was able to correlate their data to within 12%. They also proposed a model for CHF based on the suggestion by Kopchikov et al. (1969) that CHF occurs in thin films once conditions of homogeneous nucleation within the film are reached.

Sakamoto et al. (2006) suggested the heat transfer produced by arrays of nozzles might be able to be predicted from the heat transfer produced by single nozzles. They used an array of Parker Hannifin hollow-cone spray nozzles to cool a microheater array using air-saturated FC-72. The heat transfer footprint produced by a single nozzle in the array obtained by blocking off all nozzles in the spray plate except one is shown in Fig. 9. A ring of high heat transfer surrounding the spray axis is clearly observed in Fig. 5, which was found to match the region where the spray droplets impact the heater surface. TIR imaging revealed that the low heat flux region within about a 1 mm radius of the spray axis was characterized by a pool of accumulated liquid, which undergoes a process of what appears to be pool boiling at superheats above $\Delta T_{sat} > 20$ °C. Beyond the radius of predominant spray impact (approximately 2.5 mm for a 5 mm stand off), the heat flux rapidly diminishes to values on the order of 40–70 W/cm^2.

An example of the radial heat flux distribution produced by single nozzles is shown in Fig. 10. This graph was produced by plotting the heat transfer for the center 64 heaters

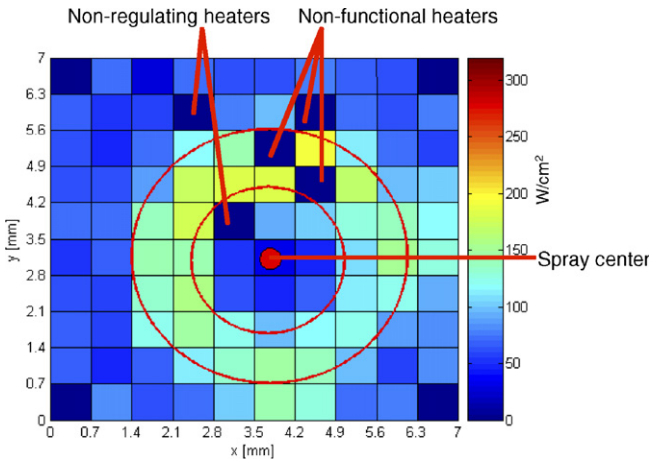

Fig. 9. Heat transfer distribution produced by a single nozzle in the array. The spray predominantly impacts the area between the two circles.

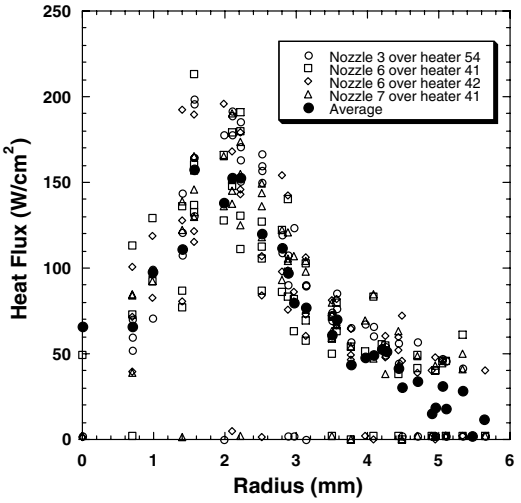

Fig. 10. Radial heat transfer profile produced by a single nozzle in the array.

in the array vs. the distance from the heater directly under the center of the spray nozzle. Data were obtained using three of the nozzles centered above the heater array and at the edge of the heater array to maximize the radial distance at which the heat flux data could be obtained. The data included the non-functional and non-regulating heaters since the surrounding heaters compensate for the locally low heat flux by dissipating commensurately more heat. The average heat transfer at each radial location is indicated by the closed circles. A library of similar curves were generated from the data taken at each wall temperature and nozzle pressure, and this single-nozzle data served as the building blocks for modeling the multi-nozzle data as discussed below. The accuracy of the radially averaged heat transfer data was checked by using it to compute the area-averaged single nozzle data and comparing it to the measured values – agreement was generally well within 10%.

An example of the heat transfer distributions produced by a 1×2 array of nozzle is shown in Fig. 11. The heat transfer in interaction zone (the area between nozzles onto which droplets from more than one nozzle strikes the surface) is higher than for single nozzle case due to the increased mass flux of liquid. The width of the interaction zone is also observed to be noticeably wider than that produced by an individual nozzle as a result of the modified liquid flux pattern caused by the overlapping sprays. Regions of low heat transfer exist in the vicinity of a given nozzle, but the location of lowest heat flux is shifted in the direction away from the interaction zone. The heaters outside the spray impact area also indicate higher heat transfer than would be expected from the single nozzle case, suggesting that more liquid is available for single or two-phase heat transfer.

The first model (Model 1) assumed that the heat transfer produced by multiple nozzles was a simple superposition of those produced by individual nozzles. The second model (Model 2) assumed that the nozzles do not interact at all, and the heat transfer surface is divided into zones of influence for each spray nozzle based on the bisector symmetry plane of the nozzles. The heat transfer in each zone was assumed to be that produced by a single nozzle. The third model (Model 3) divided the heater surface into zones of influence based on symmetry and assumed single nozzle heat transfer in each zone except within a spray interaction zone where superposition is assumed. For the current standoff distance, the interaction zone was configured to correspond with the observed region of interaction – for the 1×2 configuration this was a region 3 heaters wide and extending 7 heaters along the plane of symmetry (2.1×4.9 mm). The fourth model (Model 4) assumed the heat transfer at any location on the surface could be obtained by superposing the individual heat transfer varia-

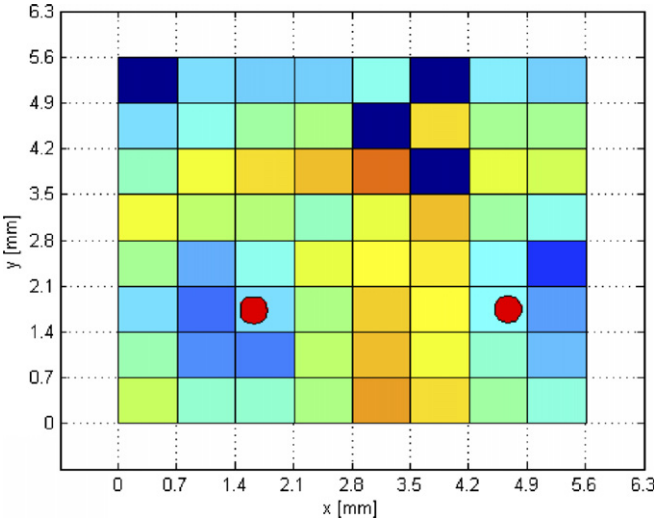

Fig. 11. Heat transfer distribution produced by a 1×2 array of nozzles ($\Delta P = 280$ kPa, $\Delta T_{sat} = 31$ °C). The nozzle locations are indicated by the red circles. (For the interpretation of colour in this figure legend, the reader is referred to the Web version of this article.)

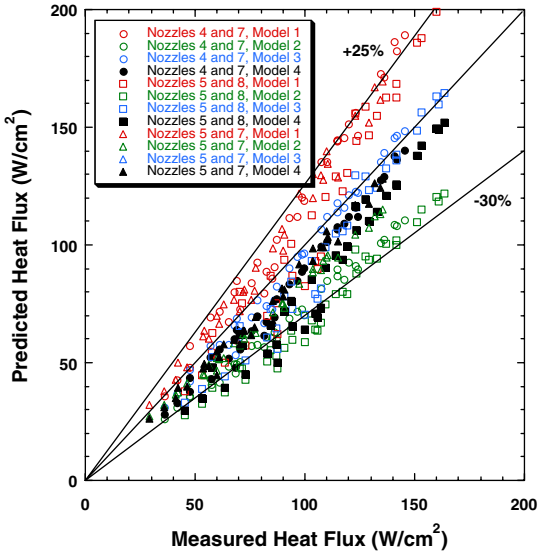

Fig. 12. Comparison of measured and predicted heat transfer distribution for 1×2 nozzle array (280 kPa, $\Delta T_{sat} = 31$ °C).

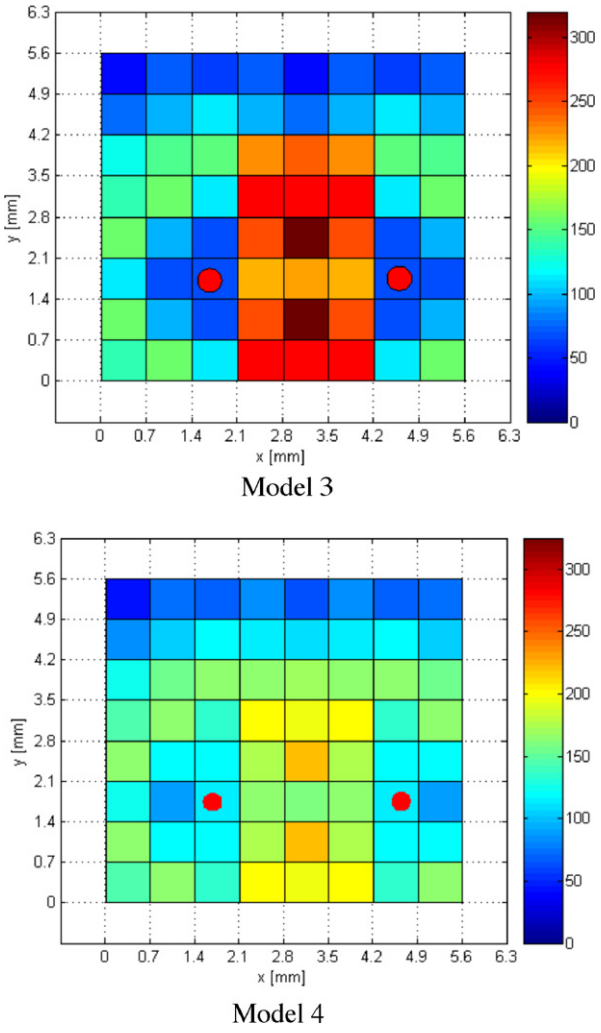

Fig. 13. Heat transfer distribution predicted by Model 3 and Model 4.

tions according to a power-law ($k = 1$ corresponds to Model 1):

$$q(r) = [q_1^k(r) + q_2^k(r) + \cdots + q_n^k(r)]^{1/k} \quad (9)$$

The results of the four models for three flow rates are summarized in Fig. 12. Model 1 overpredicted the data as might be expected, since doubling the flow rate does not double the heat transfer as the superposition model assumed. Model 2 significantly underpredicted the data since it ignores the higher heat transfer within the spray interaction zone as well as the additional flow outside the interaction zone that delays dryout of the surface. Model 3 produced very good agreement. The agreement is fortuitous, however, since the predicted heat transfer in the interaction zone is higher than the measured data indicate, and lower than the measured data in the region outside of the interaction zone as illustrated in Fig. 13. Model 3 also did not capture the shift in the location of the low heat transfer zone when another spray is present. Model 4 produced reasonably good agreement for the array averaged data and the local data for $k = 2$. It also correctly predicted the shift in the low heat flux zone under the nozzle.

6. Conclusions

Spray cooling is a very complex phenomena that is of increasing technological interest for electronic cooling and other high heat flux applications since much higher heat transfer rates compared to boiling can be achieved using relatively little fluid. The majority of the experimental data obtained to date has used heated surfaces that only allow space and time averaged heat flux and temperature to be obtained, however, and spray cooling mechanisms in both the single-phase and two-phase regimes have yet to be conclusively identified from this data. Although some prediction capabilities exist, they are generally limited to flat plate, full-cone sprays. Further advances in our understanding of spray cooling will require the development and application of new experimental techniques to measure heat transfer, film thickness, shear stress, pressure, and spray parameters, and will require the use of very high-speed videos so time-resolved images of droplet impact can be obtained.

Acknowledgements

This results presented in this work were obtained through the generous support of numerous organizations: Air Force Research Laboratory (J. Leland, R. Ponnappan, K. Yerkes), Laboratory for Physical Sciences (P. Boudreaux), NASA (E. Silk), Office of Naval Research (M. Spector), and Parker Hannifin (E. Steinthorsson).

References

Aguilar, G., Majaron, B., Popoe, K., Svaaasand, L.O., Lavernia, E.J., Nelson, J.S., 2001. Influence of nozzle-to-skin distance in cryogen

spray cooling for dermatologic laser surgery. Lasers in Surgery and Medicine 28, 113–120.

Aguilar, G., Verkruysse, W., Majaron, B., Svaasand, L.O., Lavernia, E.J., Nelson, J.S., 2001. Measurement of heat flux and heat transfer coefficient during continuous cryogen spray cooling for laser dermatologic surgery. IEEE Journal on Selected Topics in Quantum Electronics 7 (6), 1013–1021.

Aguilar, G., Wang, G.X., Nelson, J.S., 2003. Dynamic behavior of cryogen spray cooling: effects of spurt duration and spray distance. Lasers in Surgery and Medicine 32, 152–159.

Amon, C., Yao, S.C., Wu, C.F., Hsieh, C.C., 2005. Microelectromechanical system-based evaporative thermal management of high heat flux electronics. Journal of Heat Transfer 127, 66–75.

Basinger, B., Aguilar, G., Nelson, J.S., 2004. Effect of skin indentation on heat transfer during cryogen spray cooling. Lasers in Surgery and Medicine 34, 155–163.

Baysinger, K.M., Yerkes, K.L., Michalak, T.E., Harris, R.J., McQuillen, J., 2004. Design of a microgravity spray cooling experiment. In: Proceedings of the 42nd AIAA Aerospace Sciences Meeting and Exhibit, Reno, NV.

Bernardin, J.D., Stebbins, C.J., Mudawar, I., 1997. Mapping of impact and heat transfer regimes of water drops impinging on a polished surface. International Journal of Heat and Mass Transfer 40, 1996.

Bernardin, J.D., Stebbins, C.J., Mudawar, I., 1997. Effects of surface roughness on water droplet impact history and heat transfer regimes. International Journal of Heat and Mass Transfer 40, 1996.

Cader, T., Westra, L.J., Eden, R.C., 2004. Spray cooling thermal management for increased device reliability. IEEE Transactions on Device and Materials Reliability 4 (4), 605–613.

Chen, J.C., 1966. Correlation for boiling heat transfer to saturated fluids in convective flow. Industrial and Engineering Chemistry Process Design and Development 5 (3), 322–339.

Chen, R.H., Chow, L.C., Navedo, J.E., 2002. Effects of spray characteristics on critical heat flux in subcooled water spray cooling. International Journal of Heat and Mass Transfer 45, 4033–4043.

Chen, R.H., Chow, L.C., Navedo, J.E., 2004. Optimal spray characteristic in water spray cooling. International Journal of Heat and Mass Transfer 47, 5095–5099.

Chen, R.H., Tan, D.S., Lin, Juo-Chi, Chow, L.C., Griffin, A.R., Rini, D.P., 2005. Droplet and bubble dynamics in saturated FC-72 spray cooling. In: Proceedings of the 2005 ASME IMECE, Olrando, FL.

Coursey, J., Kim, J., Kiger, K.T., 2006. Spray cooling of high aspect ratio open microchannels. In: Proceedings of ITHERM 2006, San Diego, CA.

Demiray, F., Kim, J., 2004. Microscale heat transfer measurements during pool boiling of FC-72: effect of subcooling. International Journal of Heat and Mass Transfer 47, 3257–3268.

di Marzo, M., Tartarini, P., Liao, Y., Evans, D., Baum, H., 1993. Evaporative cooling due to a gently deposited droplet. International Journal of Heat and Mass Transfer 36, 4133–4139.

Estes, K.A., Mudawar, I., 1995. Correlation of Sauter mean diameter and critical heat flux for spray cooling of small surfaces. International Journal of Heat and Mass Transfer 38 (16), 2985–2996.

Estes, K.A., Mudawar, I., 1995. Correlation of Sauter mean diameter and critical heat flux for spray cooling of small surfaces. International Journal of Heat and Mass Transfer 38 (16), 2985–2996.

Ghodbane, M., Holman, J.P., 1991. Experimental study of spray cooling with Freon-113. International Journal of Heat and Mass Transfer 34 (4/5), 1163–1174.

Horacek, B., Kim, J., Kiger, K., 2004. Spray cooling using multiple nozzles: visualization and wall heat transfer measurements. IEEE Transactions on Device and Materials Reliability 4 (4), 614–625.

Horacek, B., Kiger, K., Kim, J., 2005. Single nozzle spray cooling heat transfer mechanisms. International Journal of Heat and Mass Transfer 48 (8), 1425–1438.

Hsieh, C.C., Yao, S.C., 2006. Evaporative heat transfer characteristics of a water spray on micro-structured silicon surfaces. International Journal of Heat and Mass Transfer 49, 962–974.

Kim, J.H., You, S.M., Choi, U.S., 2004. Evaporative spray cooling of plain and microporous coated surfaces. International Journal of Heat and Mass Transfer 47, 3307–3315.

Kopchikov, I., Voronin, G., Kolach, T., Labuntsov, D., Lebedev, P., 1969. Liquid boiling in a thin film. International Journal of Heat and Mass Transfer 12, 791–796.

Lee, J., Kim, J., Kiger, K., 2000. Droplet cooling heat transfer model validation. SAE Transactions Journal of Aerospace 109 (Section 1), 925–931.

Lee, J., Kim, J., Kiger, K.T., 2001. Time and space resolved heat transfer characteristics of single droplet cooling using microscale heater arrays. International Journal of Heat and Fluid Flow 22, 188–200.

Lee, J., Kiger, K.T., Kim, J., 2002. Enhancement of droplet heat transfer using dissolved gases. SAE Transactions Journal of Aerospace, 736–746.

Lin, L., Ponnappan, R., 2003. Heat transfer characteristics of spray cooling in a closed loop. International Journal of Heat and Mass Transfer 46, 3737–3746.

Lin, L., Ponnappan, R., Yerkes, K., Hager, B., 2004. Large area spray cooling. In: 42nd AIAA Aerospace Sciences Meeting and Exhibit, Reno, Nevada, pp. 10838–10843.

Liu, G.W., Morsi, Y.S., Clayton, B.R., 2000. Characterisation of the spray cooling heat transfer involved in a high pressure die casting process. International Journal of Thermal Science 39, 582–591.

Milke, J.A., Tinker, S.C., diMarzo, M., 1997. Effect of dissolved gases on spray evaporative cooling with water. Fire Technology, 2nd Quarter 33 (2).

Monde, M., Kusuda, H., Uehara, H., 1980. Burnout heat flux in saturated forced convection boiling with two or more impinging jets. Transactions of the JSME 46, 1834–1843.

Mudawar, I., Estes, K.A., 1996. Optimizing and predicting CHF in spray cooling of a square surface. Journal of Heat Transfer 118, 672–679.

Ortiz, L., Gonzalez, J.E., 1999. Experiments on steady-state high heat fluxes using spray cooling. Experimental Heat Transfer 12, 215–233.

Pais, M., Tilton, D., Chow, L., Mahefky, E., 1989. High heat flux, low superheat evaporative spray cooling. In: Proceedings of the 27th AIAA Aerospace Sciences Meeting, Reno, NV.

Pais, M.R., Chow, L.C., Mahefkey, E.T., 1992. Surface roughness and its effects on the heat transfer mechanism in spray cooling. Journal of Heat Transfer 114, 211–219.

Pautsch, A.G., Shedd, T.A., 2006. Adiabatic and diabatic measurements of the liquid film thickness during spray cooling with FC-72. International Journal of Heat and Mass Transfer 49, 2610–2618.

Pautsch, A.G., Shedd, T.A., 2005. Spray impingement cooling with single- and multiple-nozzle arrays. Part I: Heat transfer data using FC-72. International Journal of Heat and Mass Transfer 48, 3167–3175.

Qiao, Y.M., Chandra, S., 1997. Experiment on adding a surfactant to water drops boiling on a hot surface. Proceedings of the Royal Society of London Series A 453, 673–689.

Qiao, Y.M., Chandra, S., McCahan, S., 2000. Enhanced boiling of water droplets containing dissolved gases or solids. Paper No. NHTC 2000-12249, National Heat Transfer Conference, Pittsburgh, PA, August 20–22.

Rini, D.P., Chen, R.H., Chow, L.C., 2002. Bubble behavior and nucleate boiling heat transfer in saturated FC-72 spray cooling. Journal of Heat Transfer 124, 63–72.

Rybicki, J.R., Mudawar, I., 2006. Single-phase and two-phase cooling characteristics of upward-facing and downward-facing sprays. International Journal of Heat and Mass Transfer 29, 5–16.

Sakamoto, H., Kim, J., Kiger, K., Steinthorrson, E., 2006. Multinozzle spray cooling: effects of spray interaction. In: Proceedings of the 13th International Heat Transfer Conference, Sydney, Australia.

Schwarzkof, J., Cader, T., Okamoto, K., Li, B.Q., Ramaprian, B., 2004. Effect of spray angle in spray cooling thermal management of electronics. In: Proceedings of the ASME Heat Transfer/Fluids Engineering Summer Conference, Charlotte, NC, pp. 423–431.

Sehmbey, M.S., Pais, M.R., Chow, L.C., 1990. Effect of surface material properties and surface characteristics in evaporative spray cooling. In:

AIAA/ASME 5th Joint Thermophysics and Heat Transfer Conference, AIAA 90-1728, Seattle, WA.

Shedd, T.A., Pautsch, A.G., 2005. Spray impingement cooling with single- and multiple-nozzle arrays. Part II: Visualization and empirical models. International Journal of Heat and Mass Transfer 48, 3176–3184.

Silk, E., Kim, J., Kiger, K.T., 2004. Investigation of enhanced surface spray cooling. In: Proceedings of the ASME IMECE, Anaheim, CA, Paper No. IMECE2004-61753.

Silk, E.A., Kim, J., Kiger, K., 2005. Effect of spray cooling trajectory on heat flux for a straight finned enhanced surface. In: Proceedings of the ASME 2005 Heat Transfer Summer Conference, San Francisco, CA.

Stodke, C., Stephan, P., 2005. Spray cooling heat transfer on micro-structured surfaces. In: 6th World Conference on Experimental Heat Transfer, Fluid Mechanics, and Thermodynamics, Matsushima, Miyagi, Japan.

Tilton, D.E., 1989. Spray cooling. Ph.D. Dissertation, University of Kentucky.

Tilton, D.E., Tilton, C.L, Pais, M.R., Morgan, M.J., 1992. High-flux spray cooling in a simulated multichip module. In: Proceedings of the 1992 ASME Heat Transfer Conference, HTD-206-2.

Toda, S., 1974. A study of mist cooling (1st Report: Theory of mist cooling and its fundamental experiments). Heat Transfer – Japanese Research 3, 1–44.

Wayner, P., 1999. Long range intermolecular forces in change of phase heat transfer (1998 Donald Q. Kern Award Review). In: ASME/AICHE National Heat Transfer Conference Paper #320, Albuquerque, NM, August 15–17.

Yang, J., Chow, L.C., Pais, M.R., 1996. Nucleate boiling heat transfer in spray cooling. Journal of Heat Transfer 118, 668–671.

Yoshida, K., Abe, Y., Oka, T., Mori, Y., Nagashima, A., 2001. Spray cooing under reduced gravity conditions. Journal of Heat Transfer 123, 309–318.

Zhirnov, V.V., Cavin, R.K., Hutchby, J.A., Bourianoff, G.I., 2003. Limits to binary logic switch scaling – a Gedanken model. Proceedings of the IEEE 91 (11), 1934–1939.